Progress In Electromagnetics Research C, Vol. 172, 1–6, 2026

PIER C

(Received 22 January 2026, Accepted 12 June 2026, Scheduled 24 July 2026)

Cylindrical Conformal Electrically Small Antenna with Quasi-Isotropic Radiation Pattern for Mine Gob Communication

Qiushou Liu[1], Kunshan Mo[1,2,*], Jin Wu[1], Lin Peng[1,3], and Rui Fang[4]

[1] *Key Laboratory of Microwave and Optical Wave Application Technology of Guangxi Education Department Guilin University of Electronic Technology, Guilin 541004, Guangxi, China*
[2] *School of Artificial Intelligence, Guilin University of Aerospace Technology, Guilin 541004, Guangxi, China*
[3] *Nanning Guidian Electronic Technology Research Institute Co., Ltd., Nanning 530000, China*
[4] *Sichuan Technology Innovation Center for Intelligent Sensing & Computing Chip and System, China*

ABSTRACT: Wireless communication nodes in the underground mine gob area are often disturbed by different orientations; therefore, antennas with quasi-isotropic radiation are critical for reliable wireless communication. To address this challenge, a compact, cylindrical, conformal, quasi-isotropic antenna operating in the VHF band is proposed. The design integrates a shorted-patch structure with orthogonal dipole radiation, formed by a shorting post and patch aperture, to realize nearly isotropic radiation. A capacitive coupling feed is employed to enhance impedance matching, yielding an impedance bandwidth of about 1.02 MHz ($S_{11} < -10$ dB) at 170 MHz. The fabricated prototype, with dimensions of 120 mm × 120 mm × 110 mm ($0.068\lambda_0 \times 0.068\lambda_0 \times 0.063\lambda_0$), was validated through full-wave simulations and experimental testing. The two results show excellent agreement, demonstrating a measured maximum–minimum gain variation of only 2.74 dB, confirming the antenna's good quasi-isotropic characteristics. Owing to its compact volume, stable matching, and consistent omnidirectional coverage, the proposed antenna is a good candidate for underground mine gob area communication nodes.

1. INTRODUCTION

Flammable gas and ambient temperature monitoring for underground mine gob area safety are critical to preventing explosions and hazardous events, while sensor data must be reliably transmitted in real time to surface-level monitoring systems [1–3]. Nevertheless, equipment in gob areas (goafs) is often inaccessible after deployment, and antennas are prone to tilt or overturn due to shocks, collapses, or debris impacts. Therefore, for reliable underground communication, antennas with quasi-isotropic radiation are essential.

When electromagnetic waves propagate underground, rocks and soil behave as lossy media, inducing strong absorption and attenuation during transmission. Moreover, absorption and attenuation become more pronounced with increasing frequency. Conversely, conventional antennas require larger physical dimensions at lower operating frequencies — given that the typical element size is approximately 0.5λ. However, the maximum deployable antenna size is constrained by the narrow gaps pieces of mining machinery in underground coal mines, as shown in Fig. 1. When the antenna size is reduced below 0.5λ, its radiation efficiency degrades as the electrical size decreases. Therefore, after a comprehensive trade-off between antenna dimensions and operating frequency, a communication frequency of 170 MHz was selected for this research, with the antenna featuring a cross-section less than 14 cm and an overall length under 20 cm.

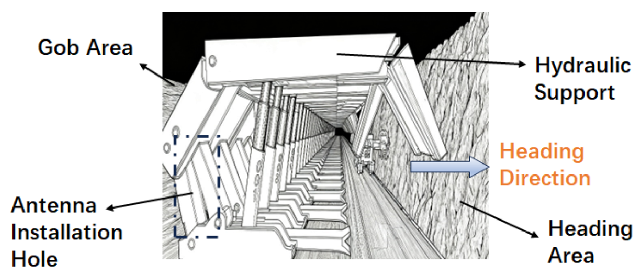

FIGURE 1. Antenna deployment schematic diagram.

Several approaches have been explored for realizing quasi-isotropic radiation. The first involves bent-dipole structures that improve current uniformity but suffer from design complexity and efficiency loss [4, 5]. The second utilizes orthogonal electric, magnetic, or complementary dipoles with controlled amplitude and phase to generate nearly spherical radiation patterns [6–14]. The third employs switched or synthesized antenna arrays, which provide flexible coverage but introduce considerable circuit complexity [15, 16]. Among them, the second method offers the most promising balance of performance and simplicity.

Accordingly, this work proposes a cylindrical conformal electrically small antenna that achieves quasi-isotropic radiation by combining orthogonal dipoles formed by the shorting post and patch aperture. A capacitive ring-slot feed improves impedance matching, while the conformal hollow shell inte-

* Corresponding author: Kunshan Mo (mks@guat.edu.cn).

doi:10.2528/PIERC26012204

Published by THE ELECTROMAGNETIC ACADEMY

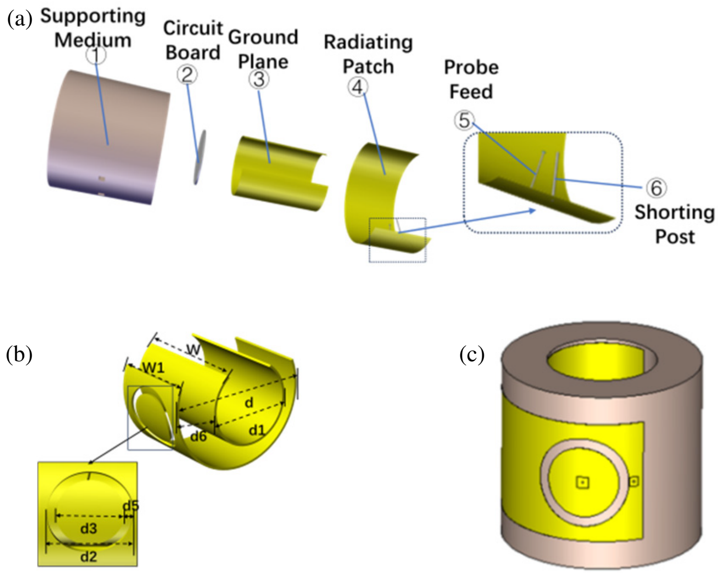

FIGURE 2. Antenna structure diagram: (a) Exploded view of the antenna structure, (b) side view of the antenna without the dielectric cylinder, and (c) overall structure diagram of the antenna.

grates communication circuits internally [17–19], maintaining a compact form factor. A prototype was fabricated and validated. The antenna achieves a 1.02 MHz bandwidth with a maximum–minimum gain variation of only 2.74 dB. These results demonstrate the antenna's effectiveness in supporting robust, maintenance-free, and space-efficient communication for mine safety monitoring systems.

2. DESIGN AND SIMULATION RESULTS

To reduce antenna size and achieve impedance matching, capacitive coupling feeding is employed. This paper proposes a short-circuited patch antenna with a cylindrical conformal ring-coupled feeding structure, where the shorting post is equivalent to a horizontal dipole, and the antenna opening is equivalent to a vertical dipole. These two mutually perpendicular and orthogonal dipoles enable the antenna's quasi-isotropic radiation in free space. It operates at 170 MHz with a bandwidth of 1.2 MHz, and the difference between the maximum and minimum power densities is 2.65 dB, with an external dimension of $120\,\text{mm} \times 120\,\text{mm} \times 110\,\text{mm}$ ($0.068\lambda_0 \times 0.068\lambda_0 \times 0.063\lambda_0$), where λ_0 refers to the free-space wavelength at the resonant frequency of the antenna.

2.1. Antenna Structure

The geometric configuration and dimensions of the antenna are illustrated in Figs. 2(a)–(c). The proposed antenna is a cylindrically conformal electrically small short-circuited patch antenna.

The proposed antenna comprises five components (Parts 1, 3, 4, 5, and 6), as shown in the exploded view of Fig. 2(a). Part 1 is a cylindrical supporting barrel made of polycarbonate (PC) material, with a thickness of 27 mm and a relative permittivity of 2.9 ± 0.5. Parts 3 and 4 are flexible polyimide plates (0.1 mm thick, $\varepsilon_r = 3.3 \pm 0.1$) printed with rectangular copper sheets. Parts 5 and 6 are connected by metallic copper pillars to form the structure in Fig. 2(b), while the complete antenna assembly is shown in Fig. 2(c).

2.2. Simulation Results and Analysis

Based on the above structural design, modeling was conducted in simulation software, and optimization of the parameters was carried out. To improve the antenna's impedance matching performance, this paper employs circular ring slot capacitive coupling feeding. Fig. 3(a) presents the reflection coefficients for different widths of the circular ring capacitive slot, with the slot width increasing from 0 mm to 8 mm. When the antenna has no capacitive coupling slot, its resonance point lies above the frequency band. When the antenna is provided with a capacitive coupling slot, it resonates at 167 MHz, but its S_{11} is higher than -10 dB. As the slot width increases, the antenna's resonant frequency gradually shifts to 170 MHz, with the resonance depth becoming progressively deeper, ultimately achieving matching at 170 MHz.

Increasing the width of the ground plane helps reduce the antenna's resonant frequency. At the same time, it also affects bandwidth to a certain extent. Fig. 3(b) shows the simulated reflection coefficients for different widths of the ground plane under the condition of slot-coupled feeding. It can be observed that as the ground plane width increases from 75 mm to 105 mm, the antenna's resonant frequency rapidly shifts downward from 179 MHz to 170 MHz, because an increase in the ground plane size expands the distribution range of image currents on its surface, lengthens the equivalent current path, and thus results in a downward shift of the frequency. However, since changes in the current path also affect the antenna's distribution of radiated power density and radiation directivity, the ground plane should be appropriately selected and adjusted.

Table 1 lists the final optimized parameters of the proposed antenna. At the resonant frequency $f_r = 170$ MHz, the antenna's current conduction and radiation characteristics show

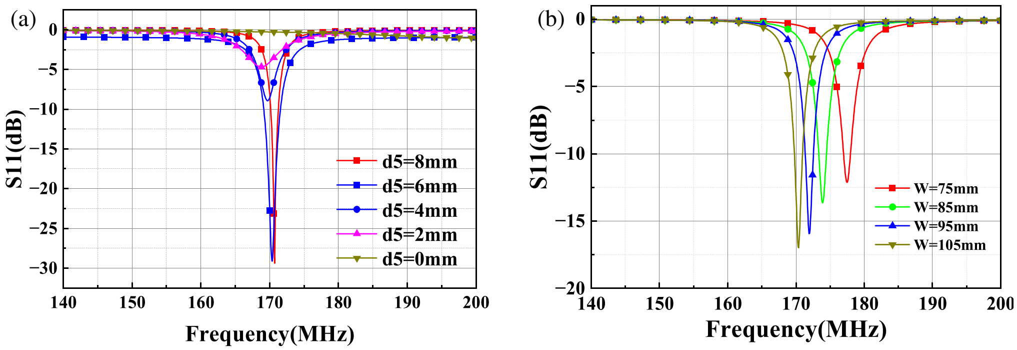

FIGURE 3. Antenna parameter sweep results diagram: (a) Simulated reflection coefficients corresponding to different slots and (b) simulated reflection coefficients for different widths of the ground plane.

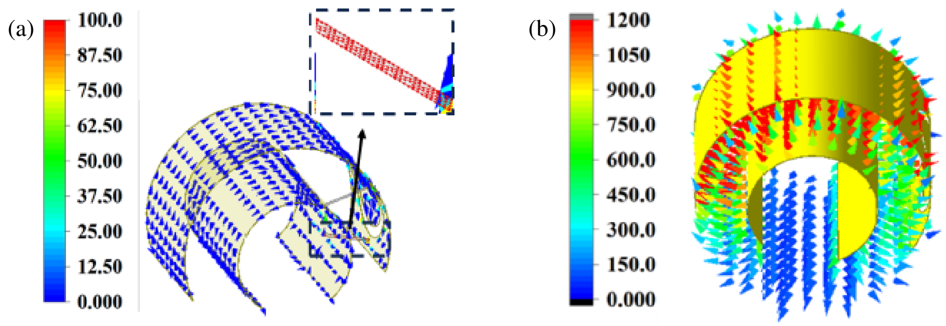

FIGURE 4. Field distribution at the resonant frequency $f = 170$ MHz: (a) Surface current and (b) electric field.

TABLE 1. Antenna structural parameters.

Parameter	Value (mm)	Parameter	Value (mm)
W	105	$W1$	75
d	120	$d1$	66
$d2$	56	$d3$	44
$d5$	6	$d6$	27

clear patterns. As shown in Fig. 4(a), the current mainly gathers on the surface of the shorted patch and flows to the ground plane through the shorting post to form a closed loop. Then, the induced currents form an equivalent magnetic-dipole radiation component, while the aperture field provides a complementary electric-dipole-like component, where surface electric currents on the shorting wall and equivalent magnetic currents at the open aperture jointly determine the radiation pattern [20]. However, since the patch's surface area is larger than that of the ground plane, this characteristic directly affects the antenna's gain balance.

In terms of details of field distribution, the antenna's electric and magnetic fields exhibit orthogonal and ordered distribution characteristics: the direction of the electric field is perpendicular to the planes of the patch and ground plane, as shown in Fig. 4(b), which forms an electric dipole to supplement the gap in magnetic dipole radiation. Therefore, the magnetic and electric dipoles radiate a quasi-isotropic pattern.

The antenna's 3D radiation pattern at 170 MHz is shown in Fig. 5. Specifically, Fig. 5(a) presents the antenna's total gain; Fig. 5(b) displays the antenna's X-polarization gain pattern, which is mainly generated by the surface current's radiation on the antenna's grounding post; Fig. 5(c) shows the Y-polarization gain pattern, formed by the radiation of the vertical magnetic current at the antenna's aperture; and Fig. 5(d) is the Z-polarization gain pattern. It can be observed that the Z-polarization gain is much smaller than the X and Y polarization gains and thus can be neglected. From the X and Y polarization gain patterns shown in Figs. 5(b) and 5(c), it can be observed that the two polarization components exhibit complementary radiation behavior, enabling the antenna to radiate in all spatial

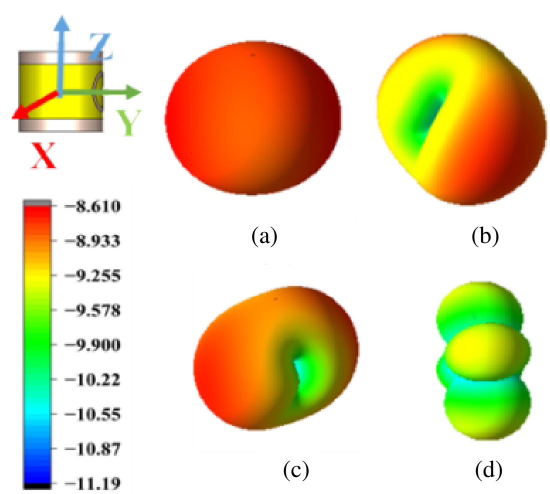

FIGURE 5. 3D radiation patterns of the antenna at 170 MHz: (a) Total gain, (b) X-polarization gain, (c) Y-polarization gain, and (d) Z-polarization gain.

directions. The antenna achieves a maximum gain of -8.62 dB along the Y-axis, while the minimum gain of -11.19 dB is observed along the x-axis. The radiation intensity in the XOZ plane is relatively uniform, and the radiation pattern is symmetric about the XOZ plane. The overall radiation gain difference of the antenna is 2.64 dB.

3. EXPERIMENTAL RESULTS AND DISCUSSION

3.1. Measured Reflection

The testing scenario and fabricated prototype of the antenna are shown in Fig. 6. The reflection coefficient measurement was conducted using a vector network analyzer.

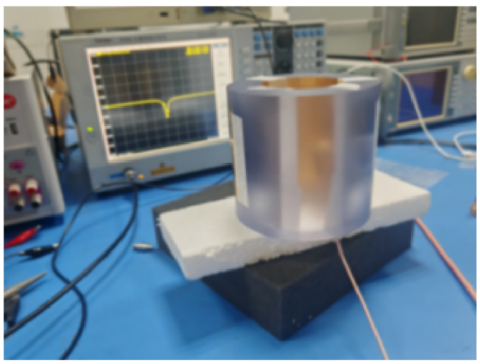

FIGURE 6. Scene diagram of antenna actual measurement.

A comparison between the simulated and measured S_{11} results is presented in Fig. 7. It can be observed that the antenna's measured results are generally consistent with the simulated ones. The simulated and measured -10 dB impedance bandwidths are approximately 1.3 MHz and 1.02 MHz, respectively. The minor discrepancy between the two results is primarily attributed to fabrication tolerances in the dielectric substrates and metal patterns, as well as slight environmental disturbances during the measurement process.

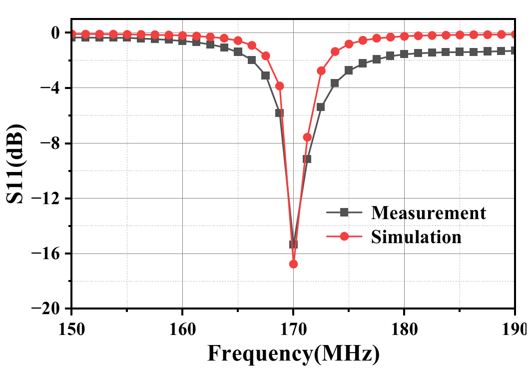

FIGURE 7. Comparison of measured and simulated S_{11} parameters.

3.2. Pattern Measurements

Since the proposed antenna operates at 170 MHz in the VHF band, and an anechoic chamber capable of reliable measurements at such a low frequency was not available, the measurements were conducted in an open field that met the required conditions, as illustrated in Fig. 8. According to the Rayleigh criterion, the far-field condition that must be satisfied for antenna radiation pattern measurements is given as follows:

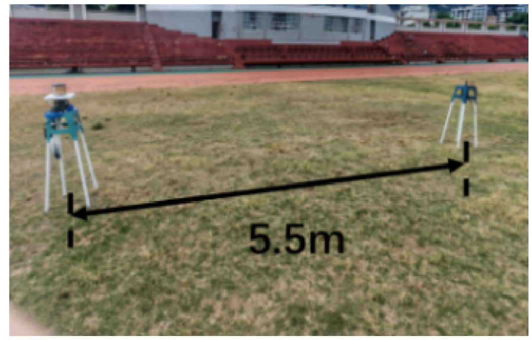

FIGURE 8. Photo of the radiation pattern measurement setup.

$$R > \frac{2D^2}{\lambda} \tag{1}$$

Substituting the diameter of the antenna's circumscribed sphere, the calculated Fraunhofer distance is 1.84 m. However, due to the small size and low gain of the electrically small antenna, its radiation pattern exhibits significant peak-valley fluctuations [21]. The test distance is therefore extended to 5.5 m to mitigate such effects. To reduce radiation pattern distortion caused by ground reflection, the antenna under test is elevated to 1.5 m [22]. Meanwhile, absorbing materials are placed between the antenna and the turntable to avoid interference from the turntable's metal components on the radiation pattern [23].

A linearly polarized rod antenna serves as the test antenna to measure the vertical and horizontal polarization electric field intensities of the proposed antenna in the XOY, XOZ, and YOZ planes, respectively. The measured field intensities are then superimposed using the following formula:

$$|E(\theta,\phi)| = \sqrt{|E_\theta(\theta,\phi)|^2 + |E_\phi(\theta,\phi)|^2} \tag{2}$$

The measured antenna radiation patterns are presented in Fig. 9. Experimental observations confirm the presence of quasi-isotropic radiation characteristics. The measured difference between the maximum and minimum radiation power densities is 2.74 dB, which is in good agreement with the simulated result of 2.67 dB. The isotropic radiation pattern remains stable across the entire passband.

Furthermore, the quasi-isotropic radiation pattern remains stable across the entire operating bandwidth, indicating that the antenna maintains consistent radiation characteristics within the target frequency range. This stability is crucial for practical applications requiring uniform signal coverage regardless of antenna orientation.

To further demonstrate the antenna advantages in the VHF band, Table 2 presents a performance comparison with several state-of-the-art communication antennas. As shown, the proposed antenna exhibits notable benefits in terms of miniaturization and reduced variation between the maximum and minimum radiation power densities, confirming its suitability for compact, orientation-insensitive deployments.

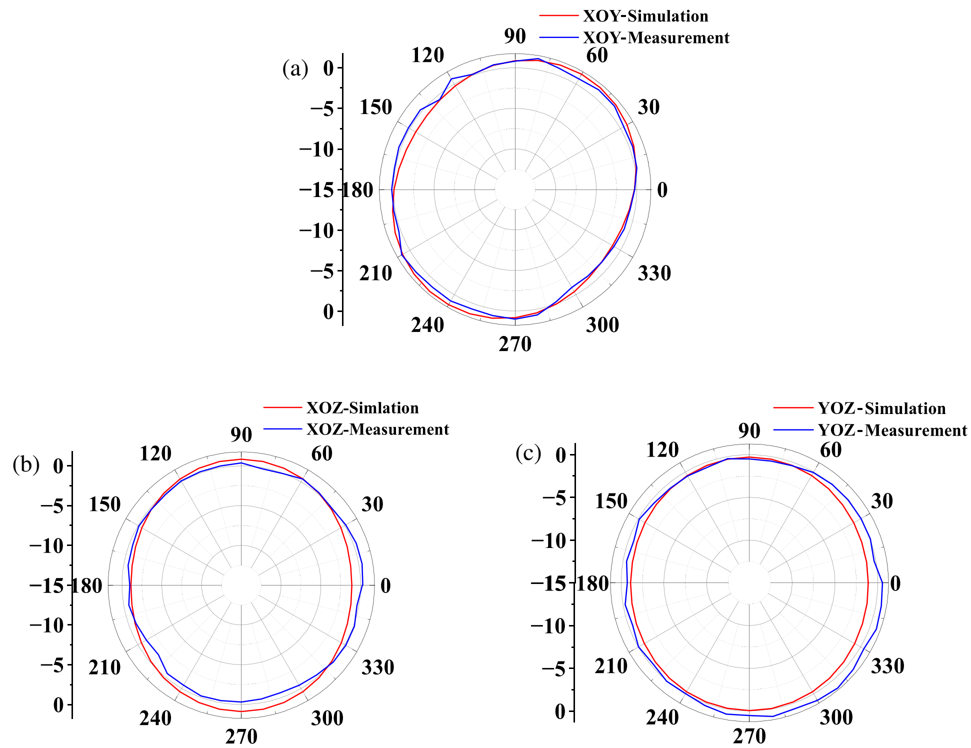

FIGURE 9. Comparison of measured and simulated antenna radiation patterns: (a) XOY plane radiation pattern, (b) XOZ plane radiation pattern, and (c) YOZ plane radiation pattern.

TABLE 2. Performance comparison between the communication antenna in this paper and advanced communication antennas.

Ref.	Year	Frequency (MHz)	Size (λ_0^3)	Gain difference	Radiation pattern
[5]	2010	911	$0.076 \times 0.076 \times 0.076$	-	quasi-isotropic
[6]	2017	2450	$0.38 \times 0.38 \times 0.048$	5.7 dB	quasi-isotropic
[7]	2020	2940	$0.45 \times 0.17 \times 0.0025$	2.9 dB	quasi-isotropic
[8]	2021	2450	$0.127 \times 0.1 \times 0.1$	3.53 dB	quasi-isotropic
[15]	2014	2400	$0.216 \times 0.216 \times 0.116$	5.6 dB	quasi-isotropic
[19]	2017	403/915/2450	$0.034 \times 0.013 \times 0.013$ $0.075 \times 0.030 \times 0.030$ $0.2 \times 0.08 \times 0.08$	> 20 dB	omnidirectionality
[20]	2022	915	$0.3 \times 0.15 \times 0.0025$	10.8 dB	quasi-isotropic
This work	-	170	$0.068 \times 0.0.068 \times 0.063$	2.74 dB	quasi-isotropic

4. CONCLUSION

This paper has presented a cylindrical, conformal, electrically small antenna that achieves quasi-isotropic radiation through the complementary behavior of orthogonal dipoles formed by a shorted patch structure. The capacitive-coupling feed effectively improves impedance matching, ensuring stable operation within the VHF band. The antenna is miniaturized to $120 \times 120 \times 110$ mm ($0.068\lambda_0 \times 0.068\lambda_0 \times 0.063\lambda_0$), making it suitable for deployment in space-constrained environments such as underground tunnels.

Comprehensive simulations and measurements confirmed the antenna's performance. The prototype achieved $S_{11} < -10$ dB over a bandwidth of about 1.02 MHz, with a gain variation of only 2.74 dB across all directions. These results verify that the proposed design delivers consistent omnidirectional coverage while maintaining compactness and simplicity. Compared with conventional quasi-isotropic antennas, the presented design offers enhanced gain uniformity and structural integration through conformal packaging. Overall, this antenna provides a practical and reliable solution for VHF-band mine safety communication, where eliminating coverage dead zones is critical. The design methodology may also inspire future electrically small antennas requiring isotropic radiation in challenging environments.

ACKNOWLEDGEMENT

This work was supported in part by the Guangxi Natural Science Foundation under Grant Nos. 2024GXNSFDA010027 and 2026GXNSFHA00640269, in part by the National Natural Science Foundation of China under Grant Nos. 62461013 and 62461012, in part by the Nanning Science Research and Technology Development Plan Project (Central Guiding Local Science and Technology Development Fund Project) under Grant No. 20231011.

REFERENCES

[1] Cacciuttolo, C., E. Atencio, S. Komarizadehasl, and J. A. Lozano-Galant, "Internet of things long-range-wide-area-network-based wireless sensors network for underground mine monitoring: Planning an efficient, safe, and sustainable labor environment," *Sensors*, Vol. 24, No. 21, 6971, 2024.

[2] Sanmiquel, L., J. M. Rossell, and C. Vintró, "Study of Spanish mining accidents using data mining techniques," *Safety Science*, Vol. 75, 49–55, 2015.

[3] Qiang, X., G. Li, J. Hou, X. Zhang, and Y. Liu, "Intelligent safety risk analysis and decision-making system for underground metal mines based on big data," *Sustainability*, Vol. 15, No. 13, 10086, 2023.

[4] Li, J., Y. Wang, L. Zhang, B. Huang, S. Yan, and X. Chen, "A quasi-isotropic antenna with system ground plane for IoT-based smart home applications," *IEEE Internet of Things Journal*, Vol. 11, No. 8, 14 449–14 459, Apr. 2024.

[5] Ryu, H.-K., G. Jung, D.-K. Ju, S. Lim, and J.-M. Woo, "An electrically small spherical UHF RFID tag antenna with quasi-isotropic patterns for wireless sensor networks," *IEEE Antennas and Wireless Propagation Letters*, Vol. 9, 60–62, 2010.

[6] Li, Q., W.-J. Lu, S.-G. Wang, and L. Zhu, "Planar quasi-isotropic magnetic dipole antenna using fractional-order circular sector cavity resonant mode," *IEEE Access*, Vol. 5, 8515–8525, 2017.

[7] Zhang, W., Y. Li, Z. Zhou, and Z. Zhang, "Dual-mode compression of dipole antenna by loading electrically small loop resonator," *IEEE Transactions on Antennas and Propagation*, Vol. 68, No. 4, 3243–3247, Apr. 2020.

[8] Wang, Y. and S. Yan, "Design of an electrically small 3-D antenna with quasi-isotropic radiation pattern," *IEEE Antennas and Wireless Propagation Letters*, Vol. 20, No. 10, 1873–1877, Oct. 2021.

[9] Wang, Y., M.-C. Tang, D. Li, K.-Z. Hu, M. Li, and X. Tan, "Low cost, electrically small, quasi-isotropic antenna based on split ring resonator," in *2019 International Applied Computational Electromagnetics Society Symposium — China (ACES)*, 1–2, Nanjing, China, 2019.

[10] Wang, R., K. Klionovski, and A. Shamim, "An antenna with quasi-isotropic radiation pattern designed with bent dipoles," in *2023 IEEE International Symposium on Antennas and Propagation and USNC-URSI Radio Science Meeting (USNC-URSI)*, 1057–1058, Portland, OR, USA, 2023.

[11] Xu, Y., Y. Zhu, S. Wen, and Y. Dong, "Planar quasi-isotropic antenna and its implementation of filtering response," *IEEE Antennas and Wireless Propagation Letters*, Vol. 20, No. 12, 2407–2411, Dec. 2021.

[12] Liang, L. and S. V. Hum, "A low-profile antenna with quasi-isotropic pattern for UHF RFID applications," *IEEE Antennas and Wireless Propagation Letters*, Vol. 12, 210–213, 2013.

[13] Peng, L., K. Sun, X. Jiang, S.-M. Li, and C.-L. Ruan, "EZR-MZR resonators for compact low-profile omnidirectional circular-polarized antenna design," *IEEE Photonics Journal*, Vol. 9, No. 4, 1–15, Aug. 2017.

[14] Munir, M. E., M. M. Nasralla, and M. A. Esmail, "Four port tri-circular ring MIMO antenna with wide-band characteristics for future 5G and mmWave applications," *Heliyon*, Vol. 10, No. 8, e28714, 2024.

[15] Pan, Y.-M., K. W. Leung, and K. Lu, "Compact quasi-isotropic dielectric resonator antenna with small ground plane," *IEEE Transactions on Antennas and Propagation*, Vol. 62, No. 2, 577–585, Feb. 2014.

[16] Cho, Y. H. and J.-Y. Kwon, "Theoretical and numerical analyses of a quasi-isotropic antenna with almost everywhere isotropy," *IEEE Access*, Vol. 13, 135 579–135 588, 2025.

[17] Sellak, L., A. Khabba, S. Chabaa, S. Ibnyaich, V. K. L. Yong, A. Baddou, and A. Zeroual, "RBFNN-based UWB 4×4 MIMO antenna design with compact size, high isolation, and improved diversity performance for millimeter-wave 5G applications," *Physica Scripta*, Vol. 99, No. 6, 066007, 2024.

[18] Su, J., B. Li, X. Yao, B. Zhao, F. Ren, H. Zhang, and X. Wang, "A L-band high gain amplifier module using 3D SiP technology," in *2023 6th International Conference on Electronics Technology (ICET)*, 324–328, Chengdu, China, 2023.

[19] Bao, Z., Y.-X. Guo, and R. Mittra, "Single-layer dual-/tri-band inverted-F antennas for conformal capsule type of applications," *IEEE Transactions on Antennas and Propagation*, Vol. 65, No. 12, 7257–7265, Dec. 2017.

[20] Wang, Y., S. Yan, and B. Huang, "Conformal folded inverted-F antenna with quasi-isotropic radiation pattern for robust communication in capsule endoscopy applications," *IEEE Transactions on Antennas and Propagation*, Vol. 70, No. 8, 6537–6550, Aug. 2022.

[21] Capozzoli, A., C. Curcio, F. D'Agostino, and A. Liseno, "A review of the antenna field regions," *Electronics*, Vol. 13, No. 11, 2194, 2024.

[22] Rodriguez, I., H. C. Nguyen, T. B. Sorensen, and O. Franek, "Base station antenna pattern distortion in practical urban deployment scenarios," in *2014 IEEE 80th Vehicular Technology Conference (VTC2014-Fall)*, 1–6, Vancouver, BC, Canada, 2014.

[23] Talashila, R. and H. Ramachandran, "Determination of far fields of wire antennas on a PEC sphere using spherical harmonic expansion," *IEEE Antennas and Wireless Propagation Letters*, Vol. 18, No. 4, 646–650, Apr. 2019.